PHYSICAL REVIEW B **91**, 014505 (2015)

Coexistence of localized and itinerant electrons in $BaFe_2X_3$ (X = S and Se) revealed by photoemission spectroscopy

D. Ootsuki,[1] N. L. Saini,[2] F. Du,[3,4] Y. Hirata,[3] K. Ohgushi,[3,5] Y. Ueda,[3,6] and T. Mizokawa[1,2,7]

[1]*Department of Physics, University of Tokyo, Kashiwa, Chiba 277-8561, Japan*
[2]*Department of Physics, Universitá di Roma La Sapienza, Piazzale Aldo Moro 2, 00185 Roma, Italy*
[3]*Institute for Solid State Physics, University of Tokyo, Kashiwa, Chiba 277-8581, Japan*
[4]*Key Laboratory of Physics and Technology for Advanced Batteries (Ministry of Education), College of Physics, Jilin University, Changchun, 130012, People's Republic of China*
[5]*Department of Physics, Tohoku University, Sendai, Miyagi 980-8578, Japan*
[6]*Toyota Physical and Chemical Research Institute, Nagakute, Aichi 480-1192, Japan*
[7]*Department of Complexity Science and Engineering, University of Tokyo, 5-1-5 Kashiwanoha, Kashiwa, Chiba 277-8561, Japan*

(Received 14 November 2014; revised manuscript received 6 January 2015; published 13 January 2015)

We report a photoemission study at room temperature on $BaFe_2X_3$ (X = S and Se) and $CsFe_2Se_3$ in which two-leg ladders are formed by the Fe sites. The Fe $2p$ core-level peaks of $BaFe_2X_3$ are broad and exhibit two components, indicating that itinerant and localized Fe $3d$ sites coexist similar to $K_xFe_{2-y}Se_2$. The Fe $2p$ core-level peak of $CsFe_2Se_3$ is rather sharp and is accompanied by a charge-transfer satellite. The insulating ground state of $CsFe_2Se_3$ can be viewed as a Fe^{2+} Mott insulator in spite of the formal valence of +2.5. The itinerant versus localized behaviors can be associated with the stability of chalcogen p holes in the two-leg ladder structure.

DOI: 10.1103/PhysRevB.91.014505 PACS number(s): 74.25.Jb, 74.70.Xa, 79.60.−i, 74.81.−g

I. INTRODUCTION

The coexistence of itinerant superconducting phase and localized antiferromagnetic phase in $K_xFe_{2-y}Se_2$ [1–4] sheds light on the intervening coupling between the electron correlation effect and the lattice effect. When the Fe $3d$ electrons are localized and form the antiferromagnetic insulating state with high-spin Fe^{2+}, the insulating phase tends to expand due to Fe-Fe bond length increase and applies a kind of pressure to the remaining metallic region [5]. The antiferromagnetic insulating phase in $K_xFe_{2-y}Se_2$ is identified as $K_2Fe_4Se_5$ with Fe vacancy order [2,3]. On the other hand, the superconducting phase is likely to be FeSe, which is under the pressure from the expanded and insulating $K_2Fe_4Se_5$. In the insulating $K_2Fe_4Se_5$ phase, the four Fe sites with square geometry form a ferromagnetic block, which couples antiferromagnetically with neighboring blocks [3]. The transfer integrals between the neighboring blocks are reduced due to the Fe vacancy, and the Mott insulating state is realized. In the XPS study on $K_xFe_{2-y}Se_2$, two components of the Fe $2p_{3/2}$ peak are assigned to the coexisting superconducting and insulating phases in the superconducting $K_xFe_{2-y}Se_2$, while in insulating $K_xFe_{2-y}Se_2$, the Fe $2p_{3/2}$ peak consists of a single component [6]. The charge-transfer energy from Se $4p$ to Fe $3d$ is estimated to be 2.3 eV, which is smaller than the repulsive Coulomb interaction between the Fe $3d$ electrons of 3.5 eV [6]. Therefore, the insulating $K_2Fe_4Se_5$ phase with high-spin Fe^{2+} can be regarded as a Mott insulating state of charge-transfer type instead of Mott-Hubbard type, and the Se $4p$ orbitals should be taken into account to explain the magnetic interactions between the Fe spins.

Recently, another insulating Fe selenide $BaFe_2Se_3$ has been attracting much attention due to the specific quasi-one-dimensional crystal structure with Pnma space group as well as the block-type antiferromagnetic state similar to $K_2Fe_4Se_5$ [7–13]. In addition, $BaFe_2Se_3$ is predicted to be a new type of multiferroic system with magnetic and ferrielectric orders in a recent theoretical work [14], which certainly enhances the interest in the title system. In $BaFe_2Se_3$, $FeSe_4$ tetrahedra share their edges and form a two-leg ladder of Fe sites as shown in Fig. 1(a). The magnetic structure of $BaFe_2Se_3$ is similar to $K_2Fe_4Se_5$ in that four Fe spins in the two-leg ladder form a ferromagnetic block and the neighboring blocks are antiferromagnetically coupled as illustrated in Fig. 1. The two-leg ladder is distorted with shorter Fe-Fe bonds (ferromagnetic and antiferromagnetic) and longer Fe-Fe bonds (ferromagnetic and antiferromagnetic) along the ladder direction. The magnetic structure is consistent with the theoretical prediction [15]. Néel temperature reported in the literatures varies from 240 K [9] to 255 K [7,8,11]. Also the magnetic moment of $BaFe_2Se_3$ ranges from 2.1 μ_B [9] to 2.8 μ_B [7,11], depending on the growth condition, and is smaller to the value expected for high-spin Fe^{2+}. Interestingly, resistivity also depends on the growth condition. Lei *et al.* reported that resistivity exhibits activation-type temperature dependence with band gap of 0.18 eV [8]. On the other hand, one-dimensional variable range hopping was reported by Nambu *et al.*, indicating that some carriers are localized due to strong scattering effect in the quasi-one-dimensional structure [11]. In addition, coexistence of itinerant and localized electrons was recently indicated by the resonant inelastic x-ray scattering study by Monney *et al.* [12]. This observation suggests that the itinerant electrons introduced by small Fe vacancy or some other effects would be responsible for the reduction of the magnetic moment and the variable range-hopping behavior of the resistivity [11]. In contrast to $BaFe_2Se_3$, $CsFe_2Se_3$ with formal Fe valence of +2.5 is much more insulating [16]. Interestingly, Fei *et al.* have revealed that all the Fe sites have the same local environment in $CsFe_2Se_3$ by means of Mössbauer spectroscopy [16]. Below 177 K, Fe spins in the two-leg ladder of $CsFe_2Se_3$ order antiferromagnetically along the rung and ferromagnetically along the leg with magnetic moment of $\sim 1.8\,\mu_B$. Usually, Mott insulators with integer number of valence are expected to be more insulating than the mixed valence systems. The

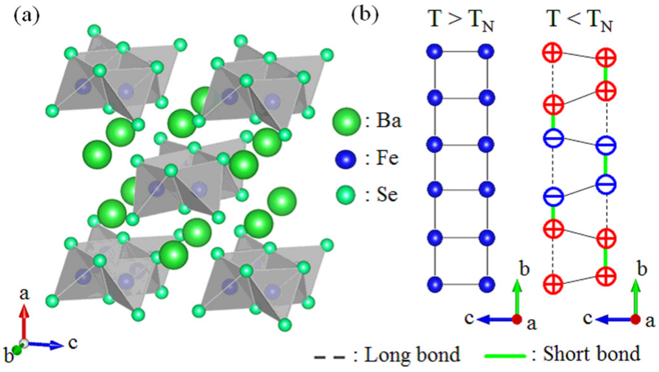

FIG. 1. (Color online) (a) Crystal structure of $BaFe_2Se_3$ visualized using the software package Vesta [18]. (b) Schematic drawing for the magnetic structure and the lattice distortion for $BaFe_2Se_3$.

situation of the two-leg ladder Fe chalcogenides is opposite to this expectation, and $CsFe_2Se_3$ with formal Fe valence of +2.5 is more insulating than integer valence $BaFe_2Se_3$ and $BaFe_2S_3$ [16]. Such puzzling mismatch between the formal valence and the transport behavior indicates unusual electronic states of the title system.

In the present work, we study fundamental electronic structures of $BaFe_2Se_3$, $BaFe_2S_3$, and $CsFe_2Se_3$ above their Néel temperatures by means of x-ray photoemission spectroscopy (XPS) and ultraviolet photoemission spectroscopy(UPS) at room temperature. The broad Fe $2p$ XPS peaks of $BaFe_2Se_3$ and $BaFe_2S_3$ indicate coexistence of localized and itinerant electrons. On the other hand, the Fe $2p$ XPS peak of $CsFe_2Se_3$ is relatively sharp, suggesting that Fe valence is homogeneous in spite of the expectation of a mixed valence state. The apparent contradiction between the valence state and the Fe $2p$ peak width can be reconciled by taking account of the Se $4p$ or S $3p$ holes.

II. EXPERIMENTS

The single crystals of $BaFe_2Se_3$, $BaFe_2S_3$, and $CsFe_2Se_3$ were grown as reported in the literatures [11,16]. We cleaved the single crystals at room temperature (300 K) under the ultrahigh vacuum for the XPS and UPS measurements. The XPS measurement was carried out at 300 K using JPS9200 analyzer. Mg Kα (1253.6 eV) was used as an x-ray source. The total energy resolution was set to ~1.0 eV. The binding energy was calibrated using the Au $4f$ core level of the gold reference sample. The UPS measurement was performed using SES100 analyzer and a He I (21.2 eV) source. The total energy resolution was set to ~30 meV and the Fermi level was determined using the Fermi edge of the gold reference sample.

III. RESULTS AND DISCUSSION

Figure 2 shows the Fe $2p$ XPS spectra of $BaFe_2Se_3$, $BaFe_2S_3$, and $CsFe_2Se_3$ taken at 300 K, which are compared with those of superconducting and nonsuperconducting $K_xFe_{2-y}Se_2$ [6]. In nonsuperconducting $K_xFe_{2-y}Se_2$, the chemical composition is close to $K_2Fe_4Se_5$ with Fe^{2+} and its ground state is a charge-transfer-type Mott insulator. The sharp Fe $2p$ peak of $CsFe_2Se_3$ is very similar to that of nonsuperconducting $K_xFe_{2-y}Se_2$ or the Fe^{2+} Mott insulator. This XPS result indicates that $CsFe_2Se_3$ would be a Mott insulator with Fe^{2+}, which is actually consistent with the Mössbauer study [16]. If all the Fe sites in $CsFe_2Se_3$ take the high-spin Fe^{2+} configuration, the extra positive charge (+0.5 per Fe) should be located at the Se sites. On the other hand, in superconducting $K_xFe_{2-y}Se_2$, itinerant Fe $3d$ electrons coexist with the localized Fe $3d$ electrons in the Mott insulating phase. The Fe $2p$ lineshape of $BaFe_2Se_3$ and $BaFe_2S_3$ is very similar to that of superconducting $K_xFe_{2-y}Se_2$, indicating coexistence of itinerant and localized electrons. In the case of superconducting $K_xFe_{2-y}Se_2$, the coexistence of the localized and itinerant electronic states is governed by the spatial distribution of the Fe vacancy. On the other hand, $BaFe_2Se_3$ and $BaFe_2S_3$ have no Fe vacancy, which can reduce transfer integrals between neighboring Fe sites and cause the Mott localization. Instead, in the two-leg ladder structure of $BaFe_2Se_3$ and $BaFe_2S_3$, the electronic interaction between neighboring Fe sites can be controlled by the Se $4p$ or S $3p$ holes, which are indicated by the mismatch between the formal valence and the transport behavior. Here, one can speculate that the Fe $3d$ electrons with the Fe^{2+} high-spin configuration and the Se $4p$ (or S $3p$) holes are localized in $CsFe_2Se_3$, whereas they are partially delocalized in $BaFe_2Se_3$ and $BaFe_2S_3$.

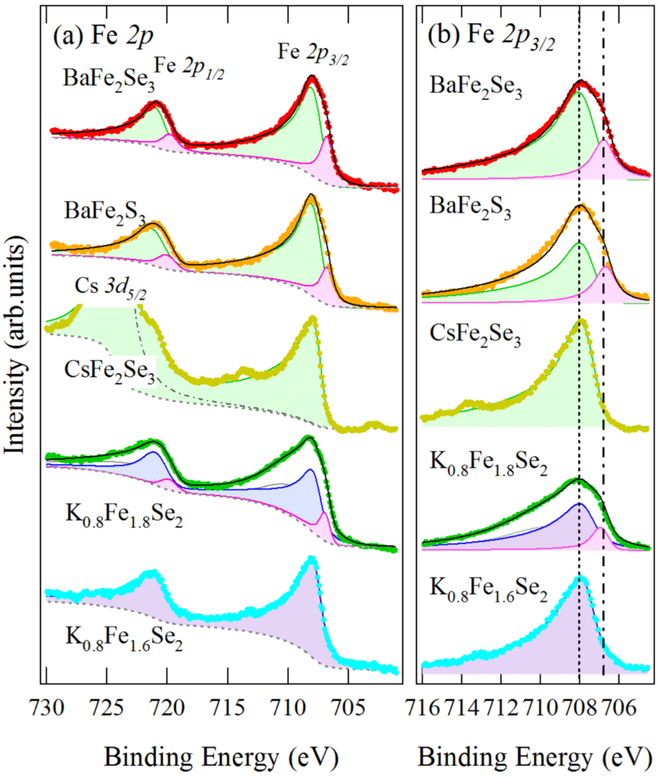

FIG. 2. (Color online) Fe $2p$ XPS of $BaFe_2X_3$ (X = S and Se) compared with $CsFe_2Se_3$ and $K_xFe_{2-y}Se_2$ (metallic and insulating) [6]. The solid curves indicate the results of curve fitting for $BaFe_2S_3$ and $BaFe_2Se_3$.

The Fe $2p_{3/2}$ and Fe $2p_{1/2}$ peaks can be decomposed into the two components, which are derived from the itinerant and localized parts. In Fig. 2, the results of Mahan's line shape fitting are indicated by the solid curves for $BaFe_2Se_3$

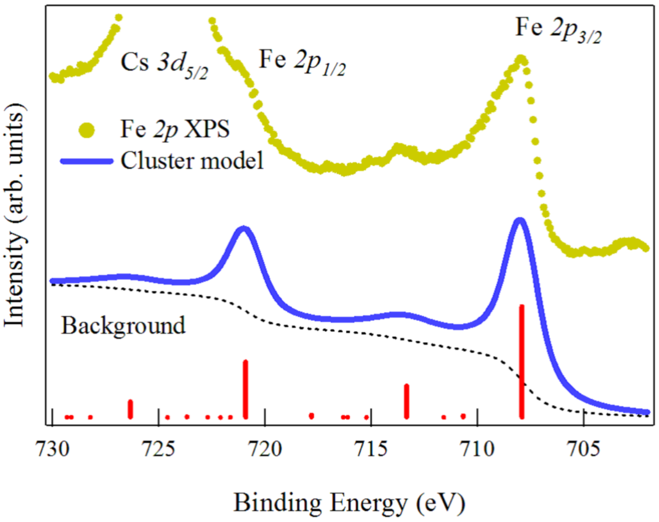

FIG. 3. (Color online) Fe $2p$ XPS of $CsFe_2Se_3$ (dots) compared with the result of cluster model calculation. The dotted curve indicates the background due to the secondary electrons.

and $BaFe_2S_3$. The itinerant component has lower binding energy due to the stronger screening effect. The intensity ratio between the itinerant and localized components is 3.0 : 5.0 for $BaFe_2Se_3$ and 2.3 : 5.0 for $BaFe_2S_3$, respectively. The relative intensity of the "itinerant" component is much larger in $BaFe_2Se_3$ and $BaFe_2S_3$ than that in $K_xFe_{2-y}Se_2$. The energy splitting between the two components is ~0.8 eV for $BaFe_2Se_3$ and $BaFe_2S_3$, which is comparable to the value for $K_xFe_{2-y}Se_2$.

Figure 3 shows the Fe $2p$ XPS of $CsFe_2Se_3$ compared with the result of the configuration interaction calculation on an $FeSe_4$ cluster model [17]. The Fe $2p_{3/2}$ peak of $CsFe_2Se_3$ (located around 708 eV) is accompanied by a broad satellite structure (located around 714 eV), which can be assigned to the charge-transfer satellite. The energy position and the intensity of the charge-transfer satellite can be analyzed using the configuration-interaction calculation on the tetrahedral $FeSe_4$ cluster model [6]. The ground state is assumed to take the high-spin d^6 state mixed with the d^7L, d^8L^2, d^9L^3, and $d^{10}L^4$ states where L represents a hole in the Se $4p$ ligand orbitals. The excitation energy from d^6 to d^7L corresponds to the charge-transfer energy Δ. The excitation energy from d^7L to d^8L^2 is given by $\Delta + U$, where U represents the Coulomb interaction between the Fe $3d$ electrons. The transfer integrals between the d^nL^m and $d^{n+1}L^{m+1}$ are described by $(pd\sigma)$ and $(pd\pi)$, where the ratio $(pd\sigma)/(pd\pi)$ is fixed at -2.16. The final states are spanned by the cd^6, cd^7L, cd^8L^2, cd^9L^3, and $cd^{10}L^4$ states, where c denotes a hole of the Fe $2p$ core level. The Coulomb interaction Q between the Fe $2p$ hole and the Fe $3d$ electron is expressed as Q, which is fixed at $U/0.8$. With $\Delta = 2.0$ eV, $U = 3.5$ eV, and $(pd\sigma) = -1.2$ eV, the calculated spectrum can reproduce the Fe $2p$ XPS result as indicated by the solid curve in Fig. 3. Δ is smaller than U, indicating that $CsFe_2Se_3$ is a Mott insulator of charge-transfer type instead of Mott-Hubbard type.

The valence-band XPS spectra of $BaFe_2Se_3$, $BaFe_2S_3$, and $CsFe_2Se_3$ taken at 300 K are displayed in Fig. 4(a) and are compared with those of superconducting and non-superconducting $K_xFe_{2-y}Se_2$ [6]. Besides the shallow core levels such as Ba $5p$, Cs $5p$, and K $3p$, the valence-band structures of the five systems are similar to one another. The spectral weight near the Fermi level increases in going from $CsFe_2Se_3$ to $BaFe_2Se_3$ to $BaFe_2S_3$, consistent with their transport properties [8,10,11,16].

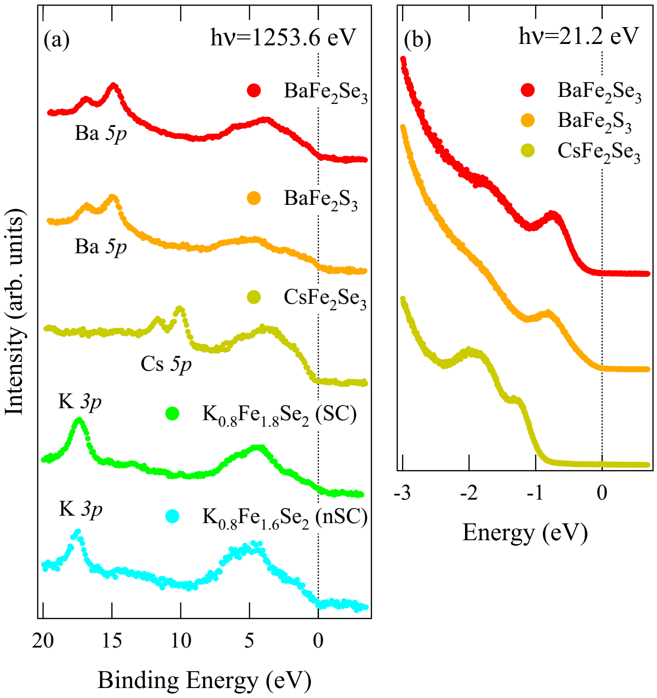

FIG. 4. (Color online) (a) Valence-band XPS of $BaFe_2X_3$ (X = S and Se) compared with $CsFe_2Se_3$ and $K_xFe_{2-y}Se_2$ (metallic and insulating) [6]. (b) UPS of $BaFe_2X_3$ (X = S and Se) compared with $CsFe_2Se_3$.

Figure 4(b) shows the UPS spectra of $BaFe_2Se_3$, $BaFe_2S_3$, and $CsFe_2Se_3$ taken at 300 K. $BaFe_2S_3$ with the highest conductivity shows the tail of the spectral weight up to the Fermi level while $BaFe_2Se_3$ has the finite band gap of ~0.2 eV. The magnitude of the band gap observed in $BaFe_2Se_3$ is more or less consistent with the activation energies obtained from temperature dependence of resistivity by Lei *et al.* [8]. $CsFe_2Se_3$ exhibits the largest band gap of ~0.8 eV, consistent with the charge-transfer-type Mott insulator deduced from the Fe $2p$ XPS result.

The apparently homogeneous Fe valence and the relatively large band gap in $CsFe_2Se_3$ can be explained based on the idea of ligand hole. The smallness of the charge-transfer energy for the Fe^{2+} state indicates that if Fe^{3+} exists in $CsFe_2Se_3$, it should take the d^6L configuration instead of d^5. In this ligand hole picture, the two-leg ladder in $CsFe_2Se_3$ accommodates the d^6-like and d^6L-like sites. Assuming that the d^6-like and d^6L-like sites are aligned along the rung, the Se $4p$ hole should be located at the Se sites sandwiched by the two legs. This situation is schematically shown in Fig. 5 where all the Fe sites take the high-spin Fe^{2+} configuration and the S $4p$ holes are localized at the Se sites on the rungs. In this scenario, the Se $4p$ holes and the Fe $3d$ electrons are partially delocalized in $BaFe_2Se_3$ and $BaFe_2S_3$ and may cause

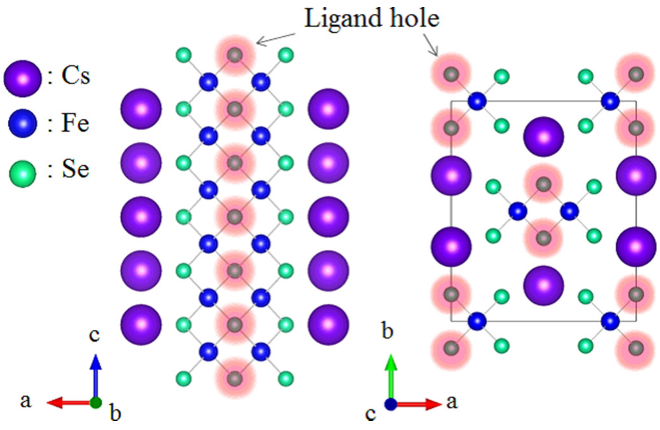

FIG. 5. (Color online) Crystal structure and possible Se $4p$ hole distribution for $CsFe_2Se_3$ visualized using the software package Vesta [18].

the lattice (and magnetic) instability. In the low-temperature phase with the lattice distortion and the block-type magnetic order, the Se $4p$ holes and the Fe $3d$ electrons would be localized in the antiferromagnetic dimer with the Fe^{2+} high-spin configuration, and they are rather "itinerant" in the ferromagnetic dimer. Here, the Se $4p$ holes and the Fe $3d$ electrons in the ferromagnetic dimer are "itinerant" in a sense that they occupy a kind of molecular orbital.

IV. CONCLUSION

In conclusion, we have studied the electronic structures of $BaFe_2X_3$ (X = S and Se) and $CsFe_2Se_3$ using photoemission spectroscopy. The Fe $2p$ core-level peaks consist of the two components in $BaFe_2X_3$, indicating that the itinerant and localized Fe $3d$ electrons coexist. The Fe $2p$ and valence-band spectra suggest that the itinerant Fe $3d$ electrons are more strongly confined in $BaFe_2Se_3$ than in $BaFe_2S_3$. On the other hand, the Fe $2p$ core-level peak of $CsFe_2Se_3$ exhibit the single component accompanied with the charge-transfer satellite. The insulating ground state of $CsFe_2Se_3$ can be viewed as a charge-transfer-type Mott insulator with localized Se $4p$ holes. In $BaFe_2X_3$ (X = S and Se), the Se $4p$ or S $3p$ holes are partially delocalized and may cause the coexistence of the itinerant and localized Fe $3d$ electrons. In future, the relationship between the chalcogen p holes, the lattice distortions, and the magnetic interactions should be further studied using various experimental and theoretical approaches.

ACKNOWLEDGMENTS

The authors thank Professors H. Takahashi, H. Okamura, and Y. Uwatoko for valuable discussions. This work was partially supported by Grants-in-Aid from the Japan Society of the Promotion of Science (JSPS) (Grant No. 25400356). D.O. acknowledges supports from the JSPS Research Fellowship for Young Scientists.

[1] J. Guo, S. Jin, G. Wang, S. Wang, K. Zhu, T. Zhou, M. He, and X. Chen, Phys. Rev. B **82**, 180520 (2010).
[2] Z. Shermadini, A. Krzton-Maziopa, M. Bendele, R. Khasanov, H. Luetkens, K. Conder, E. Pomjakushina, S. Weyeneth, V. Pomjakushin, O. Bossen, and A. Amato, Phys. Rev. Lett. **106**, 117602 (2011).
[3] F. Ye, S. Chi, W. Bao, X. F. Wang, J. J. Ying, X. H. Chen, H. D. Wang, C. H. Dong, and M. Fang, Phys. Rev. Lett. **107**, 137003 (2011).
[4] A. Ricci, N. Poccia, G. Campi, B. Joseph, G. Arrighetti, L. Barba, M. Reynolds, M. Burghammer, H. Takeya, Y. Mizuguchi, Y. Takano, M. Colapietro, N. L. Saini, and A. Bianconi, Phys. Rev. B **84**, 060511 (2011).
[5] M. Bendele, A. Barinov, B. Joseph, D. Innocenti, A. Iadecola, A. Bianconi, H. Takeya, Y. Mizuguchi, Y. Takano, T. Noji, T. Hatakeda, Y. Koike, M. Horio, A. Fujimori, D. Ootsuki, T. Mizokawa, and N. L. Saini, Sci. Rep. **4**, 5592 (2014).
[6] M. Oiwake, D. Ootsuki, T. Noji, T. Hatakeda, Y. Koike, M. Horio, A. Fujimori, N. L. Saini, and T. Mizokawa, Phys. Rev. B **88**, 224517 (2013).
[7] J. M. Caron, J. R. Neilson, D. C. Miller, A. Llobet, and T. M. McQueen, Phys. Rev. B **84**, 180409 (2011).
[8] H. Lei, H. Ryu, A. I. Frenkel, and C. Petrovic, Phys. Rev. B **84**, 214511 (2011).
[9] A. Krzton-Maziopa, E. Pomjakushina, V. Pomjakushin, D. Sheptyakov, D. Chernyshov, V. Svitlyk, and K. Conder, J. Phys.: Condens. Matter **23**, 402201 (2011).
[10] J. M. Caron, J. R. Neilson, D. C. Miller, K. Arpino, A. Llobet, and T. M. McQueen, Phys. Rev. B **85**, 180405 (2012).
[11] Y. Nambu, K. Ohgushi, S. Suzuki, F. Du, M. Avdeev, Y. Uwatoko, K. Munakata, H. Fukazawa, S. Chi, Y. Ueda, and T. J. Sato, Phys. Rev. B **85**, 064413 (2012).
[12] C. Monney, A. Uldry, K. J. Zhou, A. Krzton-Maziopa, E. Pomjakushina, V. N. Strocov, B. Delley, and T. Schmitt, Phys. Rev. B **88**, 165103 (2013).
[13] Q. Luo, A. Nicholson, J. Rincón, S. Liang, J. Riera, G. Alvarez, L. Wang, W. Ku, G. D. Samolyuk, A. Moreo, and E. Dagotto, Phys. Rev. B **87**, 024404 (2013).
[14] S. Dong, J.-M. Liu, and E. Dagotto, Phys. Rev. Lett. **113**, 187204 (2014).
[15] M. V. Medvedev, I. A. Nekrasov, and M. V. Sadovskii, JETP Lett. **95**, 33 (2012).
[16] F. Du, K. Ohgushi, Y. Nambu, T. Kawakami, M. Avdeev, Y. Hirata, Y. Watanabe, T. J. Sato, and Y. Ueda, Phys. Rev. B **85**, 214436 (2012).
[17] N. L. Saini, Y. Wakisaka, B. Joseph, A. Iadecola, S. Dalela, P. Srivastava, E. Magnano, M. Malvestuto, Y. Mizuguchi, Y. Takano, T. Mizokawa, and K. B. Garg, Phys. Rev. B **83**, 052502 (2011).
[18] K. Homma and F. Izumi, J. Appl. Crystallogr. **44**, 1272 (2011).